RESEARCH PAPER

Classification of metal PBF-LB parts manufactured with different process parameters using resonant ultrasound spectroscopy

Anne-Françoise Obaton[1] · Gregory Weaver[2] · Lucas Fournet Fayard[1] · Florian Montagner[3] · Olivier Burnet[4] ·
Alex Van den Bossche[4]

Abstract

To face the challenges raised by the qualification of metallic additively manufactured (AM) complex shaped and rough finish parts, non-destructive testing (NDT) volumetric methods are required. X-ray computed tomography (XCT) is presently the favored technique; however, alternative methods are needed to overcome the requirement of technical skills and the high cost of the technique. XCT also has limitations regarding the size and density of parts. Here, we propose an easy to use, fast, and efficient global NDT volumetric method based on resonant ultrasound spectroscopy (RUS) which basic principle relies on the comparative analysis of natural resonant frequency spectra of similar parts from the same family, both of which vibrating as free as possible. The methods have already proven to have the ability to sort parts with defects from flawless parts. In the present study, we demonstrate that RUS can also segregate metallic parts manufactured with different AM system process parameters. Eleven sets of three parts were manufactured, using a metal laser-powder bed fusion process, with different wall thicknesses, laser powers, scanning speeds, and scanning strategies. These parts were tested by RUS and then analyzed using the Z-score statistical method. The AM process parameter changes clearly influenced the resonance responses of the parts, and thus, the method is able to classify the different groups of parts according to their process parameters. Hence, the RUS methods can provide industries convenient tools to not only identify defective parts but to also configure AM machine parameters according to the expected and desired material properties.

1 Introduction

The layer wise process to build parts in additive manufacturing (AM), powder bed fusion (PBF), material jetting (MJT), vat photopolymerisation (VPP), and binder jetting (BJT)

categories of processes provides several advantages over conventional manufacturing technologies, which includes the possibility to fabricate more complex geometries, for instance, lattice or internal structures. Nevertheless, in metal AM, the as-built AM surface finish can be very rough, and like all other manufacturing methodologies, it cannot systematically produce parts that are imperfection free and compliant with

---

Recommended for publication by Commission I - Additive Manufacturing, Surfacing, and Thermal Cutting

✉ Anne-Françoise Obaton
anne-francoise.obaton@lne.fr

Gregory Weaver
gweaver@weaverndt.com

Lucas Fournet Fayard
lucas.fournetfayard@lne.fr

Florian Montagner
florian.montagner@bakerhughes.com

Olivier Burnet
olivier.burnet@grindosonic.com

Alex Van den Bossche
alex.vandenbossche@grindosonic.com

1. Laboratoire National de Métrologie et d'Essais (LNE), 1 Rue Gaston Boissier, 75015 Paris, France

2. Weaver NDT, LLC., 11035 Lavender Hill Drive, Suite 160-442, Las Vegas, NV 89135, USA

3. Baker Hughes Digital Solutions France, 68 Chemin Des Ormeaux, 69760 Limonest, France

4. GrindoSonic, Esperantolaan 4, 3001 Louvain, Belgium

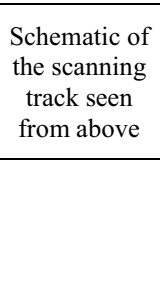**Fig. 1** **a** Numerical design and **b** photography of one of the investigated parts
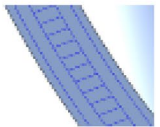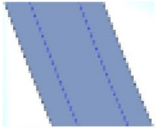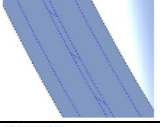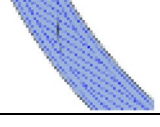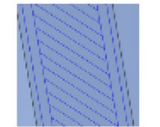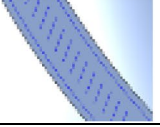

a)

b)
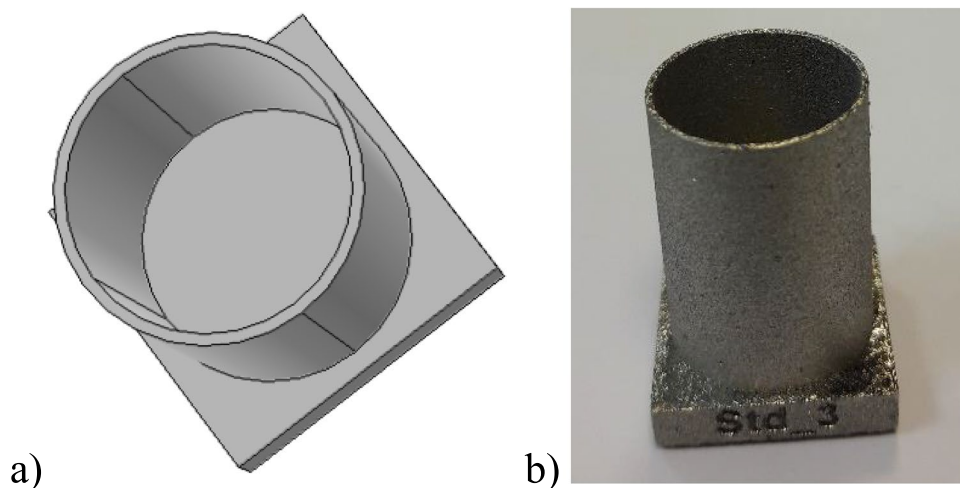
required specifications. To check the integrity of these parts, before use in their intended applications, some inspection methodologies, preferably non-destructive, are required. However, the inspection of AM parts raises numerous challenges for non-destructive testing (NDT) which is used commonly for quality assurance of parts manufactured conventionally. Indeed, some of the imperfections are specific to AM processes [1], to which should be added to the complex geometry and the roughness of the parts. The requirements of the inspection methods are that they need to be non-destructive, but also volumetric to inspect internal structures, not limited by surface roughness and/or complex shapes, and they also need to be fast and inexpensive if possible. Among the existing volumetric NDT methods, the most powerful and accepted in terms of inspection capability of complex shapes and rough surface finish part is X-ray computed tomography (XCT) [2–5]. Generally, it has enough spatial resolution to locate and even evaluate the dimensions of most internal imperfections in AM parts [6]. However, size and density of parts can be a major obstacle to the inspection. The combination of a part's density and thickness can strain the practical limitations of the XCT source power required for X-rays to fully penetrate the part. Additionally, the XCT chamber needs to be large enough to contain the entire part. XCT is also a relatively high-cost, time-consuming inspection technique that requires skilled and certified technicians to perform the testing. In addition, the resulting scan files are very large, and thus, they are not easily transferred, stored, or viewable. These disadvantages do not allow all parts to be scanned systematically. Hence, alternative non-destructive volumetric methods are required. Among all of the available non-destructive technologies, resonant ultrasound spectroscopy (RUS) [7–10] gives the most valuable results—after XCT—to control metallic parts [8, 11, 12]. RUS inspections are global or whole-body methods able
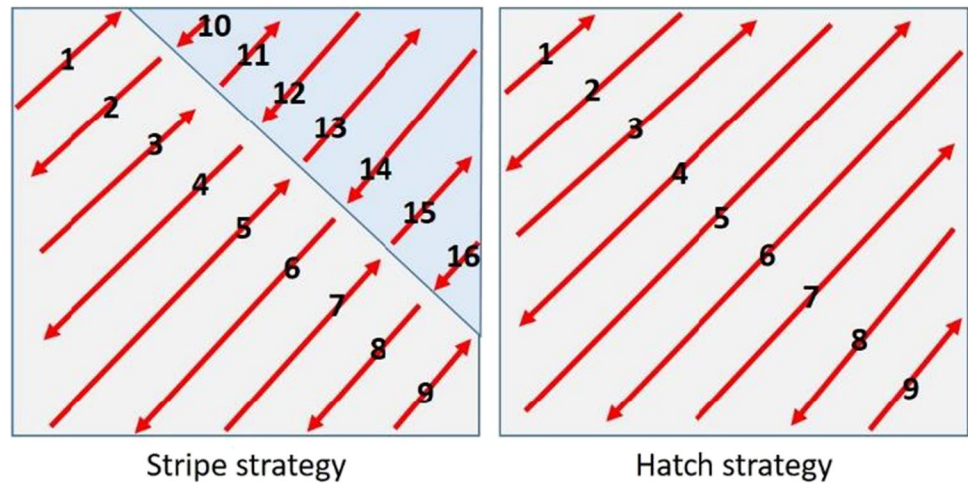
to sort parts based on the analysis of their natural resonant frequencies by comparison to the natural resonant frequencies of parts from the same family or to the modelled natural resonant frequencies. In addition to the sorting, the measurement of material elasticity constants (Young's modulus E, shear modulus G, Poisson's ratio ν, and anisotropy characteristics) of parts whose geometry is easily measurable such as bars, cylinders, tubes, and discs is possible. RUS is directly tied to the structural integrity of the parts, easy to use, fast, and exponentially affordable compared to XCT. They also can inspect any part size and shape and are insensitive to the inherent surface roughness, and they can detect material property variations that XCT cannot.

RUS is commonly used on simple geometrical specimens for defect detection or to measure the material elasticity constants [13–19]. A.S. WU et al. [20] performed a RUS parametric study into the effects of laser scanning pattern, power, speed, and build direction in powder bed fusion (PBF) AM on residual stress. Ibrahim et al. [12] used RUS to determine material properties and quality of lattice structures through the measurements of the modulus of elasticity. In our previous studies, we have evaluated RUS methods on complex AM parts containing different numbers of geometries added in their numerical design (i.e., in computed-aided design (CAD)) to simulate flaws, designated by ISO-TC261/ASTM-F42 as CAD seeded flaws, and manufactured with laser-powder bed fusion (PBF-LB) process [8, 9]. We have also investigated RUS methods on PBF-LB lattice structures with different numbers of missing struts [10, 11]. In both studies, the methods have given valuable results. The methods have been proven to be successful in the sorting of complex parts with CAD seeded flaws and/or missing struts from identical reference parts, supposedly flawless, but does the RUS method have the capability to classify parts according to

Table 1 Different process parameters or wall thickness combinations used to manufacture the investigated parts

|			Schematic of the scanning track seen from above	Wall thickness (mm)	Laser power (W)	Scanning speed (mm/s)	Laser power for contour (W)	Scanning speed for contour (mm/s)
Std1		Default parameters		0.5	253	900	180	900
Std2								
Std3								
Pb1	VED variations	Low VED		0.5	253	1875	180	900
Pb2								
Pb3								
Ph1		High VED		0.5	350	900	180	900
Ph2								
Ph3								
Pm1		Same VED as Std but different P and v		0.5	400	1425	180	900
Pm2								
Pm3								
Db1	Wall thickness variations	Very low thickness wall		0.25	253	900	180	900
Db2								
Db3								
Dm1		Low thickness wall		0.35	253	900	180	900
Dm2								
Dm3								
Dh1		High thickness wall		0.75	253	900	180	900
Dh2								
Dh3								
SH1	Scanning strategy variations	Strategy hatch instead of stripe		0.5	253	900	180	900
SH2								
SH3								
SCb1		Low scanning speed for contour		0.5	253	900	180	1,5
SCb2								
SCb3								
SCh1		High laser power for contour		0.5	253	900	253	900
SCh2								
SCh3								
S1C1		One contour instead of two		0.5	253	900	180	900
S1C2								
S1C3								

Fig. 2 Difference between stripe and hatch scanning strategies

manipulation of AM process parameters, representing as closely as possible, the potential naturally occurring flaws? In the previous study [8–11], the tested parts with CAD seeded flaws or missing struts, manufactured using PBF-LB, were compared to the reference parts, whereas in this study, we propose to classify different PBF-LB parts manufactured with different process parameters.

The paper is structured as follows: the first section describes the principle of RUS; the second section is dedicated to the presentation of the investigated metal PBF-LB parts manufactured with different process parameters; the third section reports on the experimental RUS tests and data statistical analysis of these parts. Finally, the last section presents the validation of the RUS results by comparison with experimental RUS tests with another RUS system and by XCT inspections.
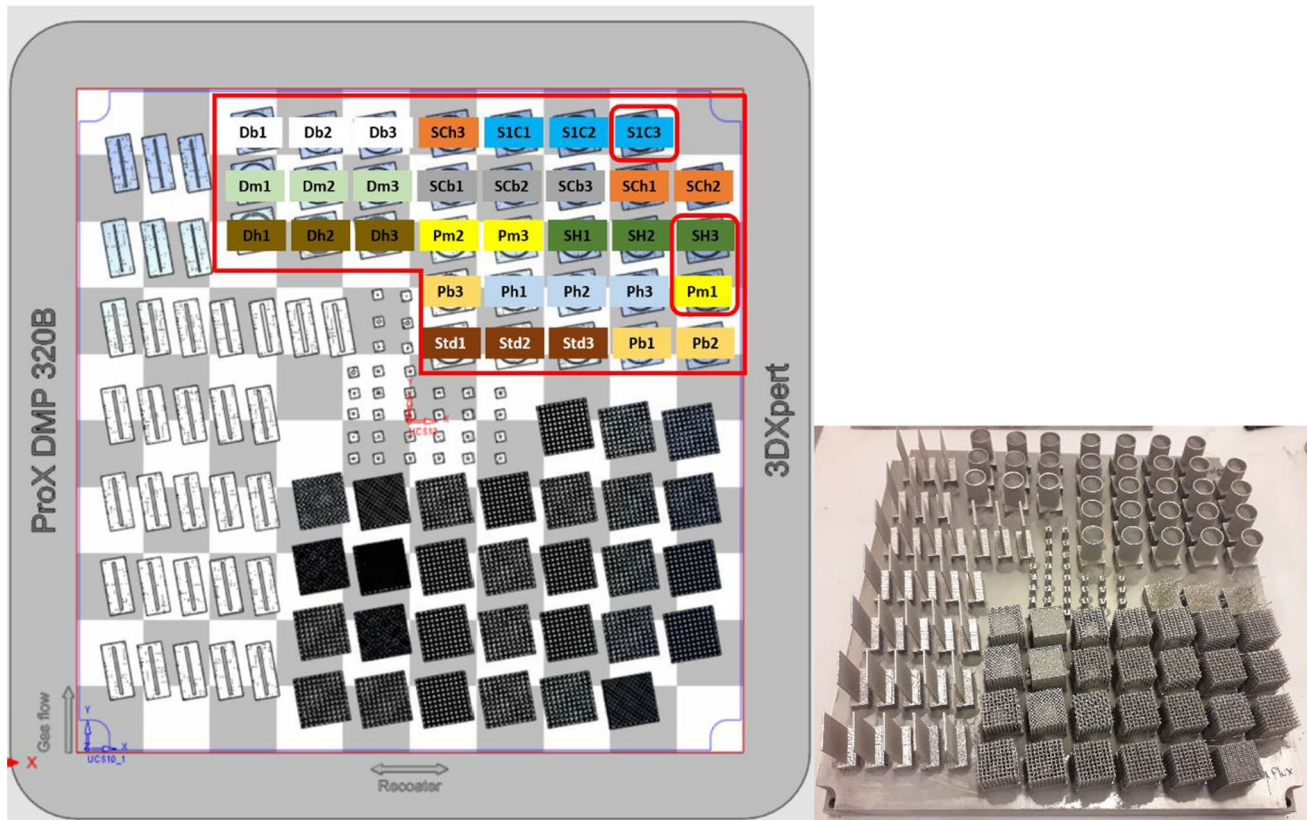
Fig. 3 Position of the investigated parts on the AM build platform: left, numerical design (the cylinders of interest are framed in red); right, photography

Fig. 4 **a** RUS IEM system installed at LNE and **b** set up configuration, including a slide, used to test the investigated parts
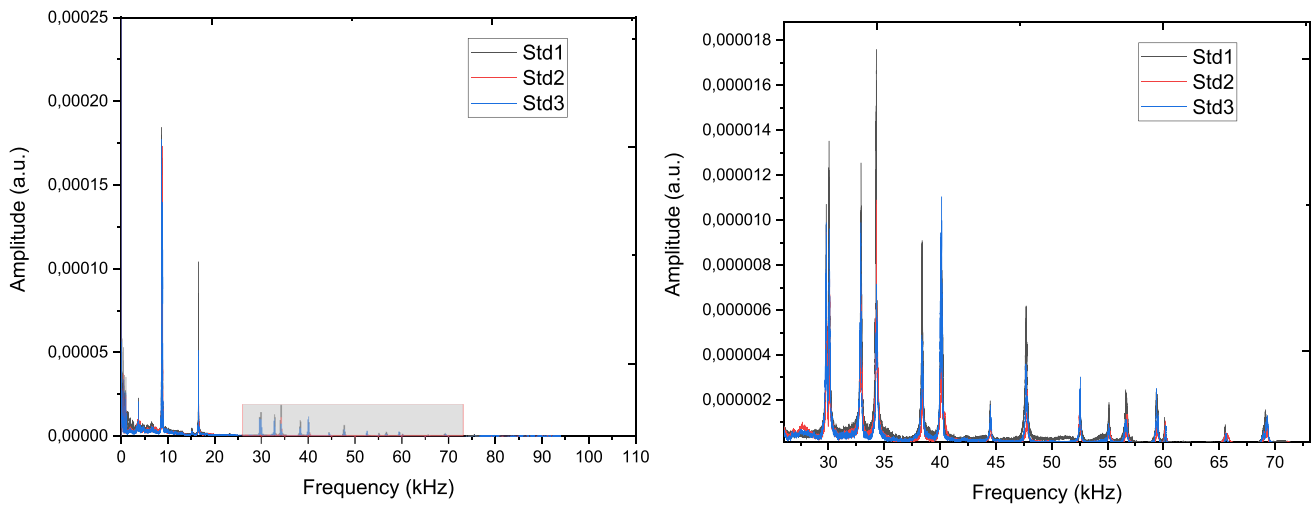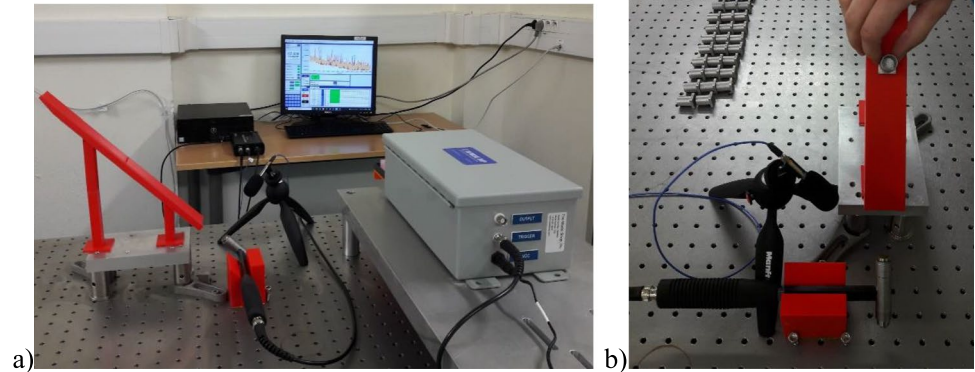
Fig. 5 Averaged frequency spectrum of the parts with default machine parameters recommended by the manufacturer (Std1-3). Right figure is a zoom of the grey zone of the left figure

2 Principle of resonant ultrasound spectroscopy (RUS)

The RUS methods are whole-body comparative inspection approaches. Their basic principle relies on the excitation of the part under test to make it vibrate as free as possible to record the natural resonant frequency spectrum of its vibrational modes and then to compare this spectrum with those of parts from the same family [21] or to modelled natural resonant frequencies. According to ASTM E2001-18 [22], there are two types of RUS methods: "swept sine method" and "impulse excitation method (IEM)." This distinction is based on the way the physical excitation of the parts under test is generated. In both cases, it is a mechanical impulse of the parts, but, in the first case, with contact piezoelectric transducers, whereas in the second case, the excitation is generated with a mechanical impulse. Then, the frequency spectrum is monitored with contact piezoelectric transducers in the case of a "swept sine

Table 2 Square root of the variances' average (σ) for the frequencies corresponding to the maximum amplitudes of the seven first peaks for each part and square root of the average of these σ (σ_{mean}) quantifying the repeatability

Part	Std1	Std2	Std3	Pm1	Pm2	Pm3	Ph1	Ph2	Ph3	Pb1	Pb2	Pb3
σ(Hz)	21	18	20	21	16	20	16	11	15	19	15	26
Part	Db1	Db2	Db3	Dm1	Dm2	Dm3	Dh1	Dh2	Dh3	SCb1	SCb2	SCb3
σ(Hz)	18	22	21	15	16	13	17	14	16	8	9	11
Part	SCh1	SCh2	SCh3	SH1	SH2	SH3	S1C1	S1C2	S1C3	All Parts		
σ(Hz)	13	18	11	19	16	16	21	19	24	σ_{mean} (Hz)		17

Fig. 6 Graphical representation of the Z-score RUS data statistical analysis over all investigated parts
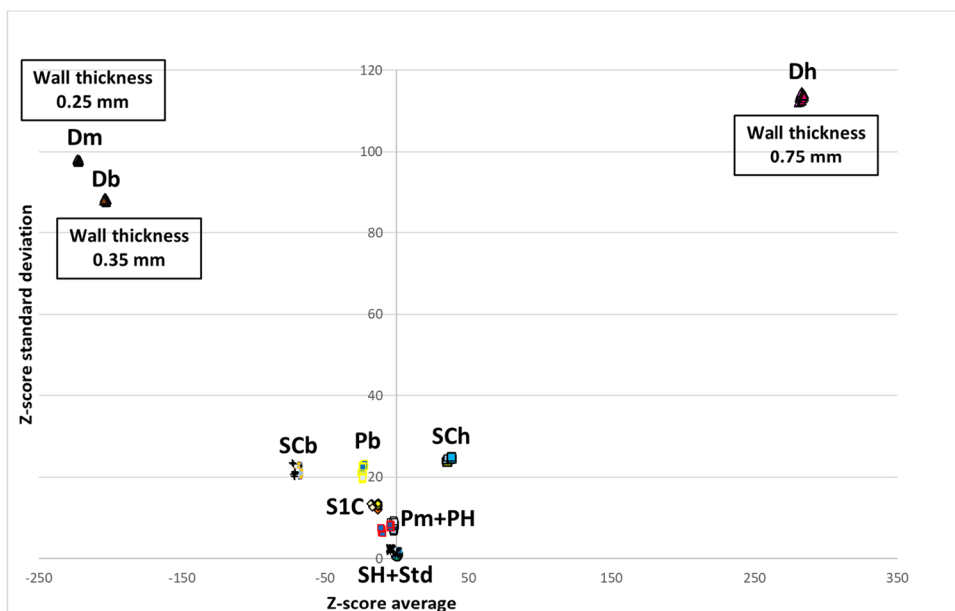

method," while it is recorded with either a microphone or a piezoelectric transducer in the case of IEM methods.

Two similar objects will have comparable resonant frequency spectra. A shift of a frequency or multiple frequencies of a tested part, compared to other parts from the same family, will be the indicator of a structural difference in the tested part: changes in its geometry, density, elasticity, or external/internal structural integrity (e.g., material alterations or imperfections and AM process deviations).

3 Additively manufactured (AM) investigated parts with different process parameters

To evaluate the influence of AM machine process parameters on the properties of additively manufactured parts, cylinder-shaped parts (Fig. 1), with different thicknesses, were fabricated implementing various laser powers, scanning speeds, and scanning strategies. These parts were then measured with a coordinate measuring machine (CMM) to assess geometrical

Fig. 7 Zoom of Fig. 6 excluding parts with different wall thicknesses
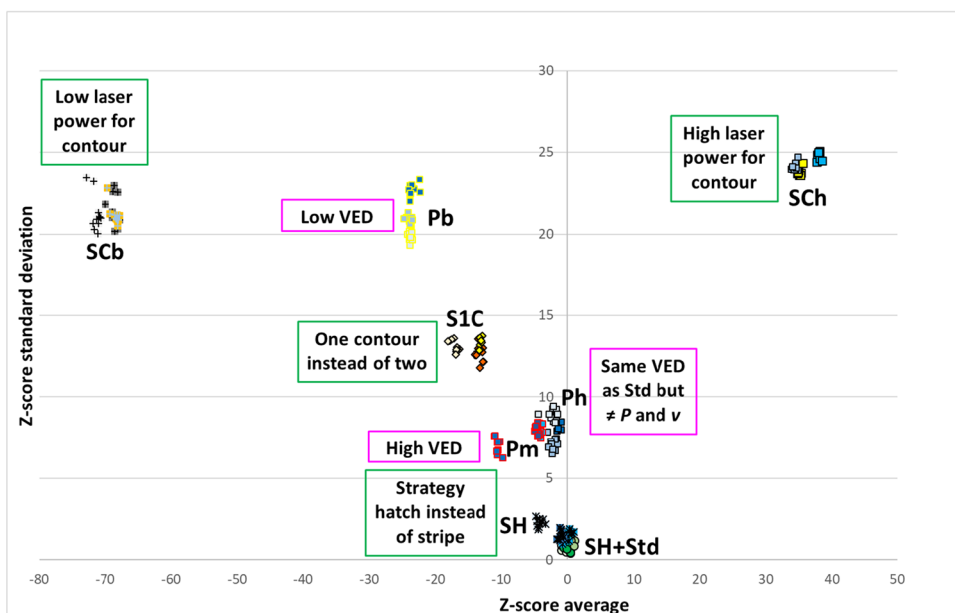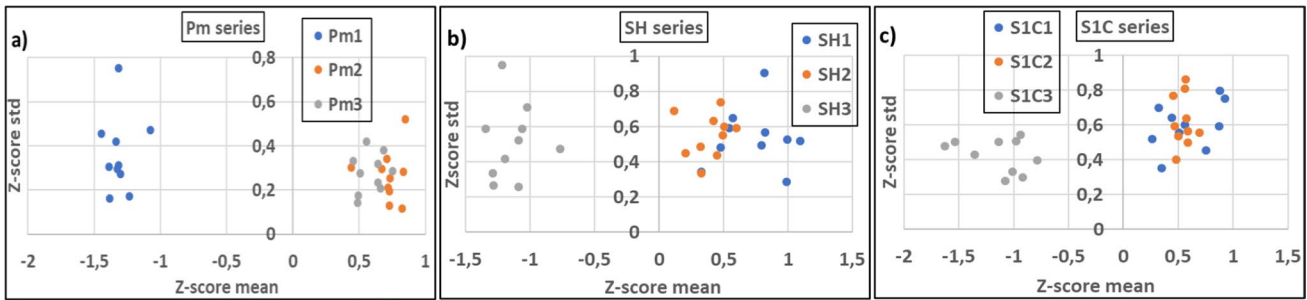
Fig. 8 Identification of the outliers among a set of parts from the same family

and dimensional deviations between the manufactured part and its CAD model. No clear information could be extracted from such measurements. Thus, it was decided to use RUS methods to determine the influence of the process parameters on the structural properties of the parts.

A cylinder of 20 mm height, 14 mm internal diameter, and different thicknesses, with a fully dense base of $17 \times 17 \times 4$ mm^3, is designed as presented in Fig. 1a.

Several cylinders were then manufactured (Fig. 1b), in Inconel 625, with a 3DSystems ProX DMP320 PBF-LB machine. The scanning strategy, for all cylinders, consisted of back and forth trajectories with a rotation of 65° between each layer and a contour step occurring after the filling step. The hatch space was set by default to be 100 μm and the layer thickness to be 60 μm. Supports were added below the bases to remove the parts easily from the build platform. The difference between the cylinders, in wall thicknesses, laser powers, scanning speeds, and scanning strategies, are synthesized in Table 1. Eleven sets of process parameters or wall thickness combinations were chosen, and three parts per combination were manufactured to check the AM process repeatability.

A set of parts with default machine parameters recommended by the PBF-LB machine manufacturer (Std) was produced. Then, the first combination of three sets was manufactured with various laser powers (P in Watt) and scanning speeds (v in mm/s) (Pb, Ph, and Pm), defined by their volumetric energy density (VED in J/mm^3):

$$VED = \frac{P}{v \times S} \quad (1)$$

where S represents the surface of the laser beam which was measured with a beam profiling camera (in mm^2).

A second combination of three sets with three different thicknesses (Db, Dm, and Dh) was manufactured, and finally, a third combination of four sets with various scanning strategies (SH, SCb, SCh, and S1C) as specified in Table 1. A stripe scanning strategy and two contour steps were chosen for all cylinders except for the set referenced SH, for which a hatching scanning strategy was chosen, and for the set referenced S1C, there is only one contour step. The difference between hatching and stripe scanning strategies is illustrated in Fig. 2.

Table 3 Assumptions that could explain the reason of outliers among a set of parts from the same family

| Outlier in a set of 3 cylinders	Position on the AM platform	Cylinders that should be XCT scanned
Pm1	Isolated from Pm2/3 and on the edge	Pm1 and Pm2 or Pm3
SH3	On the edge	SH3 and SH1 or SH2
S1C3	On the edge	S1C3 and S1C1 or S1C2
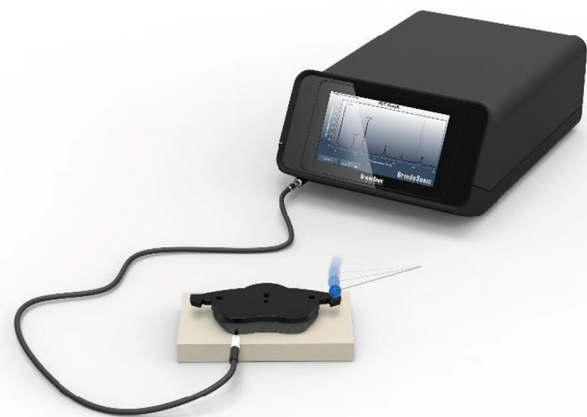
Fig. 9 RUS system from GrindoSonic used to test the investigated parts
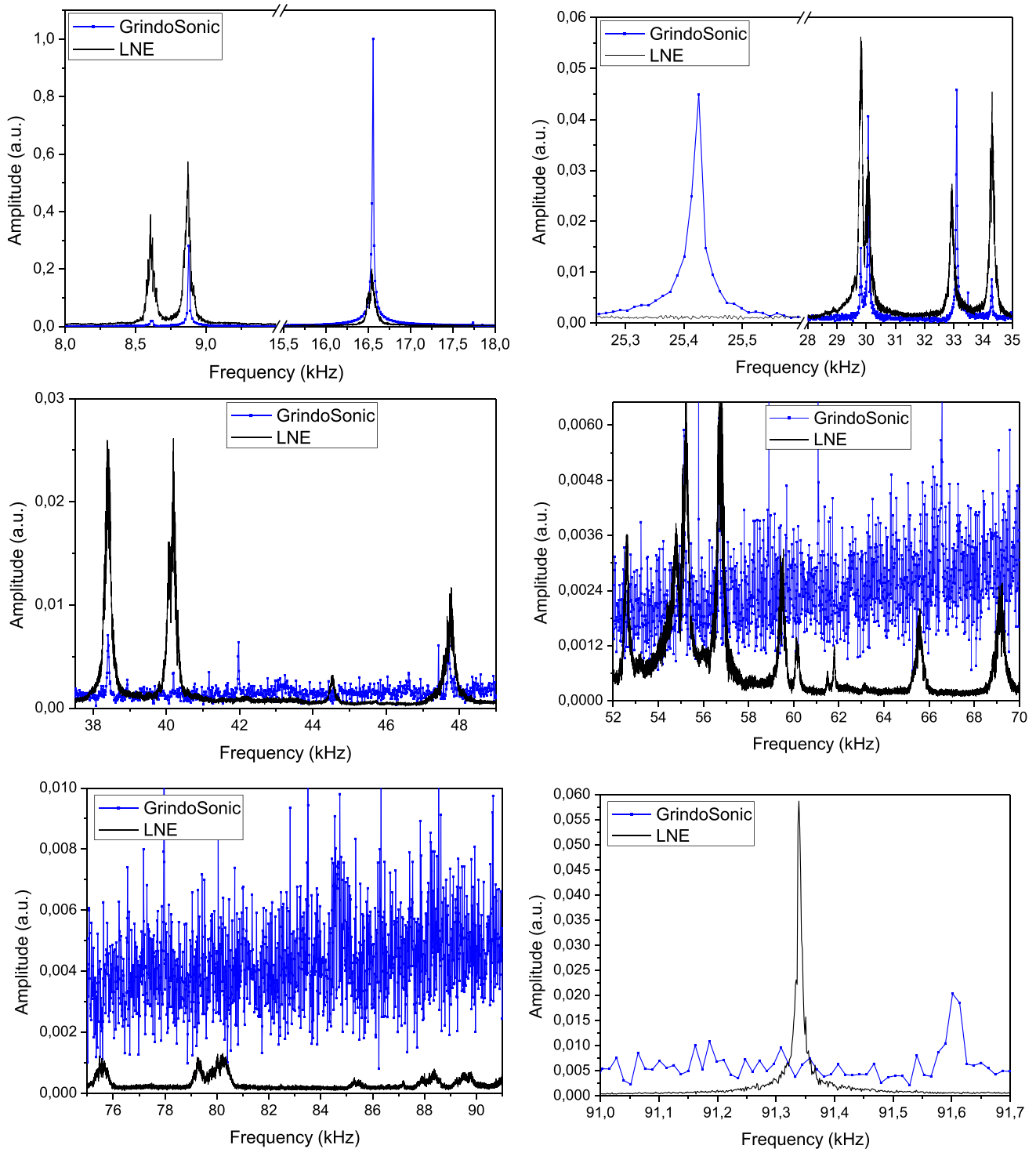
Fig. 10 Comparison of a RUS spectrum acquired by GrindoSonic and a RUS spectrum acquired by LNE on a part with default machine parameters recommended by the manufacturer (Std1) all over the frequency range

Fig. 11 Comparison, performed by GrindoSonic, of the frequency positions of the two first vibrational modes for all parts
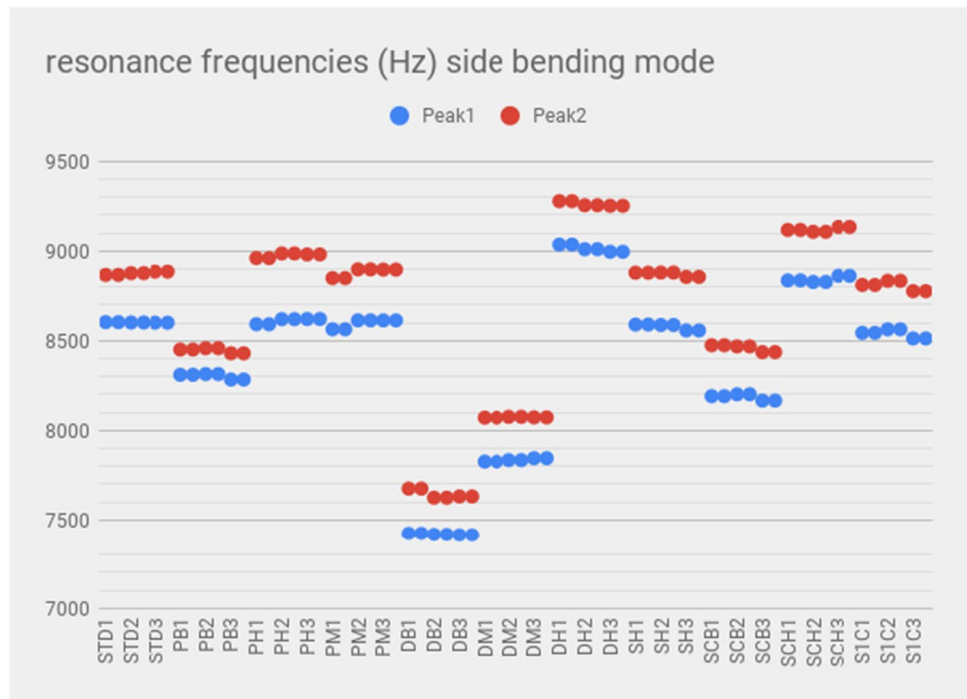
The parts were manufactured within the same batch with other parts. They were localized as illustrated in Fig. 3.

4 Experimental RUS tests on the AM investigated parts with different process parameters

4.1 RUS tests

In this study, LNE tested the parts with its IEM system (RAM-UP11HK) developed by The Modal Shop (TMS) (Fig. 4a). The system is equipped with a connected modal

Fig. 12 Waygate Technologies vltomelx m 300/180 XCT from Baker Hughes used to inspect the investigated parts

hammer, enabling the impact force to be measured, and a microphone. The output of the microphone is converted into a frequency spectrum in the range from 100 Hz to 94 kHz using a high-speed analog to digital converter (24 bits) performing a fast Fourier transform (FFT).

For these tests, to excite the cylinders, the parts were presented for impulse from a slide to the modal hammer such as shown in Fig. 4b. Each cylinder was tested and positioned similarly on the slide (reference at the bottom, cylinder perpendicular to the slide, launched from about halfway up the slide), in the frequency range of 100 Hz to 94 kHz, with the highest resolution of 1.465 Hz which gives an acquisition time of 0.683 s.

Each cylinder was tested ten separate times to allow for verification of repeatability. The overall averaged spectra for the parts with default machine parameters recommended by the manufacturer (Std1-3) is presented on Fig. 5. Table 2 gives the square root of the variances' average (σ) for the frequencies corresponding to the maximum amplitudes of the seven first peaks, for each part, as well as the square root of the average of these σ (σ_{mean}) to quantify the repeatability for separate tests and all tests.

4.2 RUS data statistical analysis

The data statistical analysis was performed by Weaver NDT using Z-score method to classify the different groups of parts within the overall parts by comparison to the set of parts with default process parameters recommended by the manufacturer (Std1-3).

Table 4 XCT parameters used to scan

Voltage (kV)	Current (μA)	Exposure time (ms)	Filter	Number of projections	Frame per projections	Reconstructed voxel size (μm × μm × μm)
180	100	334	None	2200	3	18 × 18 × 18

For each part, ten RUS tests were performed. The analysis implies the averages (*avg*) of the ten frequencies of the maxima for the seven first peaks in the whole frequency spectra. This selection is because lower frequency data are usually key to material property differences. This choice turned out to be relevant to classify all the cylinders as this is presented below.

The *Z*-score [23] was, thus, calculated from the below relation:

$$Z - \text{score} = \frac{\text{freq peak for the tested part} - \text{avg of the 30 freq peaks for the Std series}}{\text{standard deviation of the 30 freq peaks for the Std series}}$$

(2)

The *Z*-score deviation was then plotted versus the *Z*-score average for all parts as presented in Figs. 6 and 7.

These plots are particularly evocative. The AM process parameter changes clearly affect the frequency position of the resonance peaks, and one can classify the different set of three parts according to their process parameters. As shown in Fig. 6, the key parameter is wall thickness, and then, as shown in Fig. 7, high laser power variation for the contour is very important, more important than the one contour instead of two. A low *VED* has more impact than a high *VED*, and if the *VED* is the same as the default parameters, but with higher laser power and increased scanning speed, the impact is quite important. The type of scanning strategies (hatch or stripe) has a lower impact on the integrity of the parts. Such plots clearly show how the AM process parameter changes influence the resonance responses of the parts.

Among the Pm, SH, and S1C series, dispersion within each set is observed as highlighted in Fig. 8. Pm1, SH3, and S1C3 are outliers (Table 3). This may be because these parts are all located on the edge of the AM platform (see Fig. 3 parts framed by a red square). To identify the origins of the differences in these responses, they were
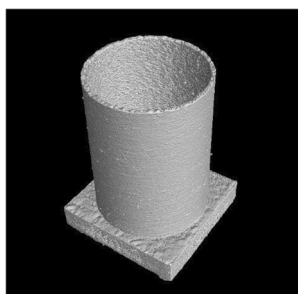
scanned with XCT to check if the deviations are resulting from internal flaws (see paragraph 5.2).

5 Validation of the experimental RUS tests on the AM investigated parts with different process parameters
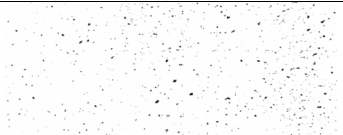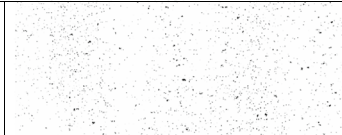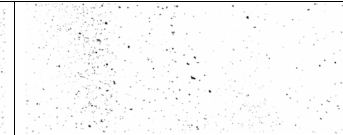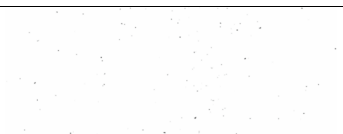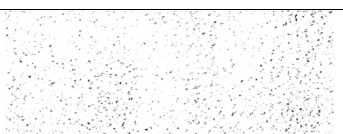
5.1 Experimental RUS tests with another RUS system

To demonstrate that the resonant frequency spectra of the tested parts are not system or operator dependent, the parts were also tested with an IEM RUS system developed and commercialized by GrindoSonic, namely, the MK7 (Fig. 9). Both methods, from TMS and GrindoSonic, include a modal hammer and a microphone. However, the excitation of the part was different in the two cases. LNE presented the parts to the TMS system from a slide to the hammer, whereas GrindoSonic hit t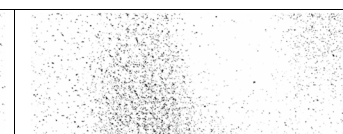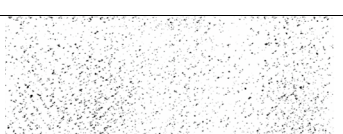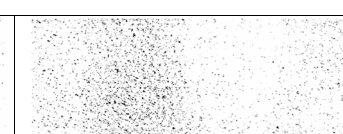he parts, in the middle of the cylinder height, laying on a foam, with the hammer such as show in Fig. 9. Two tests were performed per part as the standard deviation over ten separate tests on a part was evaluated to be 0.093 Hz on the 8.5 kHz peak.

Figure 10 shows the comparison of a RUS spectrum acquired by GrindoSonic and a RUS spectrum acquired by LNE on a part with default machine parameters recommended by the manufacturer (Std1) all over the frequency range. Most peaks below 50 kHz are located at the same frequency. However, LNE did not observe any peak around 25.4 kHz whereas GrindoSonic does. We attributed this dissimilarity to the difference in excitation between LNE and GrindoSonic, but this is still invalidated. The mode is possibly not activated by the free-falling process used by LNE. Above 50 kHz, the comparison was not possible as the range of sensitivity of the systems are different.

Figure 11 presents a comparison, performed by GrindoSonic, of the frequency positions of the two first vibrational modes for all parts. This figure confirms the statistical analysis performed by Weaver NDT on the LNE data. The highest shifts from the Std set are observed for the Dm, Db, and Dh sets, then for Pb, SCh, and SCb. A difference is also observed between Pm1, SH3, and S1C3 and the rest of their respective set.

Fig. 13 XCT image of the whole cylinder

Table 5 XCT unrolled images of three different layers in the thickness of the cylinder and porosity rate for each layer (in %)

Position (mm)	-0.15	0	+0.15	avg	std
Part's reference	Pm1 outlier				
Image					
Porosity (%)	0.809	1.537	1.942	1.43	0.47
Part's reference	Pm2				
Image					
Porosity (%)	1.260	1.413	1.012	1.23	0.17
Part's reference	SH3 outlier				
Image					
Porosity (%)	0.264	0.081	0.152	0.166	0.075
Part's reference	SH1				
Image					
Porosity (%)	0.085	0.087	0.069	0.0803	0.0080
Position (mm)	-0.15	0	+0.15	avg	std
Part's reference	S1C3 outlier				
Image					
Porosity (%)	2.570	0.971	4.376	2.6	1.4
Part's reference	S1C2				
Image					
Porosity (%)	4.455	1.293	5.095	3.6	1.7

5.2 X-ray computed tomography (XCT) inspections

In order to find an explanation of the dispersion of RUS results within a set of similar parts with identical process parameters, the outlier as well as another part from the same set was scanned by Baker Hughes using their Waygate Technologies v|tome|x m 300/180 XCT system (Fig. 12).

This 300 kV system is equipped with a micro focus source and a dyn|41–100 detector with a 100 µm pitch distance. The distance between the source and the detector (FDD, focal detector distance) is around 800 mm. The XCT parameters used to scan the parts of interest are given in Table 4, and Fig. 13 presents an XCT image of the whole cylinder.

The XCT unrolled images for Pm1/Pm2, SH3/SH1, and S1C3/S1C2 for three different layers on the cylinder element, in the center (defined as position 0 mm), and then on both borders (defined as position -0.15 and +0.15 mm from the center) are presented in Table 5. This table also gives the porosity rate (in %) for each layer.

It can be observed, either on the images or on the porosity average and/or the standard deviation, that the porosity rate or the distribution is significantly different for all outliers compared to the part from the same family. A higher

standard deviation indicates that the porosity is not evenly distributed among the parts, while a higher average indicates that the porosity rate is higher. Thus, the differences between the parts, produced with the same parameters, can be assigned to a difference in porosity levels and/or the uneven distribution of the porosity and therefore a difference in overall material modulus.

6 Conclusions

We have conducted an experimental and statistical study to investigate the feasibility of resonance ultrasound spectroscopy (RUS) to classify complex shaped and rough finished additively manufactured (AM) parts, according to their machine process parameters.

In the first section, the principle of RUS has been reported. In the second section, the AM parts have been detailed. Eleven sets of three similar cylinders with a base have been manufactured, in Inconel 625, using a laser-powder bed fusion process. Either the wall thicknesses, the laser powers, the scanning speeds, or the scanning strategies were modified in between these eleven sets. In the third section, the RUS experimental conditions have been described, the experimental results on the cylinders are provided, and their statistical analysis has been presented. The results are particularly conclusive. The method could successfully classify the different parts according to their AM process parameters. In the fourth section, the RUS results are validated using another system and operator, and the XCT inspection is documented. The other RUS system gave similar results. One single response difference was identified, and this was determined to be dependent on the method by which the part is excited. The XCT scans highlighted that the outlier within a same parameter series is attributed to location on the edge of the AM build platform and porosity distribution.

This study demonstrated that the IEM RUS methods provide qualitative results in identifying defective parts, but they also are successful in classifying parts according to their AM process parameters. The methods provide valuable benefits. They are non-destructive, volumetric, easy to use, very quick, and simple to operate, and no part preparation or fixturing is required. In addition, there is no restriction in size and shape for the test parts, and surface roughness does not prevent accurate and repeatable testing. This study has shown that RUS methods are very suitable tools for the AM industry, as an alternative to XCT, for routine quality inspections for medium to high volumes.

Declarations

References

1. Dutton B, Vesga W, Waller J, James S, and Seifi M (2020) Metal additive manufacturing defect formation and nondestructive evaluation detectability", in Structural Integrity of Additive Manufactured Parts, ASTM International., West Conshohocken. PA: Shamsaei N, Daniewicz S, Hrabe N, Beretta S, Waller J, Seifi M pp. 1–50. https://doi.org/10.1520/stp162020180136
2. Chiffre L, Carmignato S, Kruth J-P, Schmitt R, Weckenmann A (2014) Industrial applications of computed tomography. CIRP Ann-Manuf Technol 63:655–677. https://doi.org/10.1016/j.cirp.2014.05.011
3. Wits WW, Carmignato S, Zanini F, Vaneker THJ (2016) Porosity testing methods for the quality assessment of selective laser melted parts. CIRP Ann 65(1):201–204. https://doi.org/10.1016/j.cirp.2016.04.054
4. Thompson A, Maskery I, Leach RK (2016) X-ray computed tomography for additive manufacturing: a review. Meas Sci Technol 27(7):072001. https://doi.org/10.1088/0957-0233/27/7/072001
5. du Plessis A et al (2019) Laboratory X-ray tomography for metal additive manufacturing: round robin test. Addit Manuf 30:100837. https://doi.org/10.1016/j.addma.2019.100837
6. Carmignato S, Dewulf W, Leach R (2017) Industrial X-ray computed tomography. Springer
7. Todorov E, Spencer R, Gleeson SP, Jamshidinia M, and Kelly SM (2014) America makes: National Additive Manufacturing Innovation Institute (NAMII) project 1: nondestructive evaluation (NDE) of complex metallic additive manufactured (AM) Structures. https://doi.org/10.21236/ada612775
8. Obaton A-F, Butsch B, McDonough S, Carcreff E, Laroche N, Gaillard Y, Tarr J, Bouvet P, Cruz R, Donmez A (2020) Evaluation of nondestructive volumetric testing methods for additively manufactured parts", in Structural Integrity of Additive Manufactured Parts. ASTM International., West Conshohocken, PA: Shamsaei N, Daniewicz S, Hrabe N, Beretta S, Waller J, Seifi M pp. 51–91. https://doi.org/10.1520/STP162020180099
9. Obaton A-F, Butsch B, Carcreff E, Laroche N, Tarr J, Donmez A (2020) Efficient volumetric non-destructive testing methods for additively manufactured parts. Weld World 64(8):1417–1425. https://doi.org/10.1007/s40194-020-00932-0
10. McGuigan S, Arguelles A, Obaton A-F, Donmez A, Rivière J, Parisa S (2021) Resonant ultrasound spectroscopy for quality control of geometrically complex additively manufactured components. Addit Manuf 39:101808. https://doi.org/10.1016/j.addma.2020.101808

11. Obaton A-F, Wang Y, Butsch B, Huang QA (2021) Non-destructive resonant acoustic testing and defect classification of additively manufactured lattice structures. Weld World 65:361–371. https://doi.org/10.1007/s40194-020-01034-7

12. Ibrahim Y, Li Z, Davies CM, Maharaj C, Dear JP, Hooper PA (Dec.2018) Acoustic resonance testing of additive manufactured lattice structures. Addit Manuf 24:566–576. https://doi.org/10.1016/j.addma.2018.10.034

13. Migliori A, Maynard JD (2005) Implementation of a modern resonant ultrasound spectroscopy system for the measurement of the elastic moduli of small solid specimens. Rev Sci Instrum 76(121301):1–7

14. Flynn K, Radovic M (2011) Evaluation of defects in materials using resonant ultrasound spectroscopy. J Mater Sci 46:2548–2556

15. Delaunay T, Le Clézio E, Guennou M, Dammak H, Pham Thi M, Feuillard G (2008) Full tensorial characterization of PZN-12%PT single crystal by resonant ultrasound spectroscopy. IEEE Trans Ultrason Ferroelectr Freq Control. 55(2):476–488

16. Ohno I (1976) Free vibration of a rectangular parallelepiped crystal and its application to determination of elastic constants of orthorhombic crystals. J Phys Earth 24(4):355–379. Accessed: Jan. 25, 2020. [Online]. Available, https://www.jstage.jst.go.jp/article/jpe1952/24/4/24_4_355/_pdf/-char/en.

17. Demarest HH (1971) Cube-resonance method to determine the elastic constants of solids. J Acoust Soc Am 49(3B):768–775. https://doi.org/10.1121/1.1912415(Mar.)

18. Flynn K, Radovic M (2011) Evaluation of defects in materials using resonant ultrasound spectroscopy. J Mater Sci 46(8):2548–2556. https://doi.org/10.1007/s10853-010-5107-y

19. Solodov I, Bai J, Busse G (2013) Resonant ultrasound spectroscopy of defects: case study of flat-bottomed holes. J Appl Phys 113(22):223512. https://doi.org/10.1063/1.4810926

20. Wu AS, Brown DW, Kumar M, Gallegos GF, King WE (2014) An experimental investigation into additive manufacturing-induced residual stresses in 316L stainless steel. Metall Mater Trans A Phys Metall Mater Sci 45A:6260–6270

21. Obaton A-F, Van den Bossche A, Burnet O, Butsch B, Zouggarh I, Soulard F, Johnson W (2022) Novel or improved NDE inspection capabilities for additively manufactured parts," in Progress in additive manufacturing 2020. In: N. Shamsaei, M. Seifi (ed) (West Conshohocken, PA: ASTM International, STP1637). https://doi.org/10.1520/STP163720200096

22. ASTM E2001-18 (2018) Guide for resonant ultrasound spectroscopy for defect detection in both metallic and non-metallic parts. ASTM International. https://doi.org/10.1520/E2001-18

23. ISO 13528 (2015) Statistical methods for use in proficiency testing by interlaboratory comparison. https://compass.astm.org/content-search/?content=13528&stype=A